Mechanism of Olefin Hydrosilylation Catalyzed by $RuCl_2(CO)_2(PPh_3)_2$: A DFT Study†

Tell Tuttle,* Dongqi Wang, and Walter Thiel*

Max-Planck-Institut für Kohlenforschung, D-45470 Mülheim an der Ruhr, Germany

Jutta Köhler, Marco Hofmann, and Johann Weis

Consortium für Elektrochemische Industrie GmbH, Zielstattstrasse 20, D-81379 München, Germany

Received April 25, 2006

Density functional theory (DFT) was used to explore the different mechanistic possibilities for the hydrosilylation reaction between methyldimethoxysilane and methylvinyldimethoxysilane catalyzed by the Ru(II) complex dicarbonyldichlorobis(triphenylphosphine)ruthenium(II) (**A1**). Reaction enthalpy profiles of the Chalk−Harrod, modified Chalk−Harrod, and σ-bond metathesis mechanisms were computed for several different active forms of **A1**. A total of 10 different pathways with different catalytic cycles and different induction steps were compared. We predict that a σ-bond metathesis mechanism involving the formation of a hydride analogue of **A1** is most favored, in contrast to the commonly accepted Chalk−Harrod mechanism of hydrosilylation. The B3LYP-calculated activation energy within the catalytic cycle (ΔH_{act} = 21.8 kcal/mol) is small enough to make **A1** a reasonable catalyst for this reaction under the normally applied experimental conditions.

Introduction

Hydrosilylation plays a pivotal role in the manufacturing of commercially available silicon-based products: silicone rubber, liquid injection molding compounds, paper-release coatings, pressure-sensitive adhesives, binders, and coupling agents are all constructed from organo-functional silicon monomers and through cross-linking silicon polymers.[1−4] Hydrosilylation, the addition of hydrosilanes across unsaturated bonds,[2,5−7] is an important reaction in the process of creating organosilicon building blocks from which these more complex materials can be constructed.

Hydrosilylation reactions are normally performed under mild conditions in the presence of a catalyst.[2,5−7] Traditionally, the most common catalysts for these reactions have been platinum-based compounds.[2,5−8] Their predominance in the market has resulted from their high activity and the possibility of fine-tuning their activity in order to avoid unwanted side effects. Previously, we have demonstrated[8] for a particular class of platinum-based catalysts, bis(alkynyl)(1,5-cyclooctadiene)platinum complexes $(COD)Pt(CCR)_2$,[9] how the catalytic ability can be tuned in the induction phase (i.e., by controlling the type of active compound that is generated).

It is well known that other transition metal compounds can catalyze the hydrosilylation reaction, too, e.g., those based on ruthenium.[10−17] However, with these catalysts the activity and selectivity of platinum catalysts is normally not achieved since several side reactions can also occur, including olefin isomerization, dehydrogenative silylation, and hydrogenation. In the present study we focused on the ruthenium complex $RuCl_2(CO)_2(PPh_3)_2$ (**A1**), which shows reasonable hydrosilylation activity in a test reaction of diethoxymethylsilane and diethoxymethylvinylsilane (see Experimental Section).

To optimize **A1** and related ruthenium-based catalysts, it is essential to have an understanding of the mechanism by which the catalyst operates. Thus, we present in this report the results of a computational investigation to determine the mechanism by which **A1** catalyzes the reaction between dimethoxymethylsilane (**R1**) and dimethoxymethylvinylsilane (**R2**) to form 1,2-bis(dimethoxymethylsilyl)ethane (**P1**) (Scheme 1), as a step toward the fine-tuning of **A1** for optimal activity.

The commonly accepted mechanisms for the hydrosilylation of alkenes, with late transition metal catalysts, are the Chalk−

† This paper is dedicated to Prof. Siegfried Hünig on occasion of his 85th birthday.

* Corresponding authors. E-mail: thiel@mpi-muelheim.mpg.de (W.T.) and tell@mpi-muelheim.mpg.de (T.T.).

(1) Lewis, L. N.; Stein, J.; Gao, Y.; Colborn, R. E.; Hutchins, G. *Platinum Met. Rev.* **1997**, *41*, 66.

(2) Marciniec, B.; Gulinski, J.; Urbaniak, W.; Kornetka, Z. W. *Comprehensive Handbook on Hydrosilylation*; Pergamon Press: Oxford, 1992.

(3) Noll, W. *Chemistry and Technology of Silicones*; Academic Press: New York, 1968.

(4) Stark, F. O.; Falender, J. R.; Wright, A. P. In *Comprehensive Organometallic Chemistry*; Wilkinson, G., Stone, F. G. A., Abel, W. E., Eds.; Pergamon Press: Oxford, 1982; Vol. 2, p 306.

(5) Armitrage, D. In *Comprehensive Organometallic Chemistry*; Wilkinson, G., Stone, F. G. A., Abel, W. E., Eds.; Pergamon Press: Oxford, 1982; Vol. 1, p 117.

(6) Ojima, I. In *The Chemistry of Organic Silicon Compounds*; Patai, S., Rappoport, Z., Eds.; John Wiley & Sons: New York, 1989; p 1479.

(7) Speier, J. L. In *Advances in Organometallic Chemistry*; Stone, F. G. A., Abel, W. E., Eds.; Academic Press: New York, 1979; Vol. 17, p 407.

(8) Jagadeesh, M. N.; Thiel, W.; Köhler, J.; Fehn, A. *Organometallics* **2002**, *21*, 2076.

(9) Fehn, A., Achenbach, F., Appl., E. P., Eds.; *Curable Silicone Rubber Compositions Containing Organoplatinum Catalysts*; Wacker-Chemie G.m.b.H.: Germany, 2000; Vol. EP 994159.

(10) Beddie, C.; Hall, M. B. *J. Am. Chem. Soc.* **2004**, *126*, 13564.

(11) Glaser, P. B.; Tilley, T. D. *J. Am. Chem. Soc.* **2003**, *125*, 13640.

(12) Chung, L. W.; Wu, Y. D.; Trost, B. M.; Ball, Z. T. *J. Am. Chem. Soc.* **2003**, *125*, 11578.

(13) Trost, B. M.; Ball, Z. T. *J. Am. Chem. Soc.* **2003**, *125*, 30.

(14) Trost, B. M.; Ball, Z. T. *J. Am. Chem. Soc.* **2001**, *123*, 12726.

(15) Maruyama, Y.; Yamamura, K.; Sagawa, T.; Katayama, H.; Ozawa, F. *Organometallics* **2000**, *19*, 1308.

(16) Ojima, I.; Fuchikami, T.; Yatabe, M. *J. Organomet. Chem.* **1984**, *260*, 335.

(17) Maruyama, Y.; Yamamura, K.; Nakayama, I.; Yoshiuchi, K.; Ozawa, F. *J. Am. Chem. Soc.* **1998**, *120*, 1421.

10.1021/om060359h CCC: $33.50
Publication on Web 08/17/2006

Scheme 1. Chemical Structure and Notation of the Reactants, Products, and Catalyst

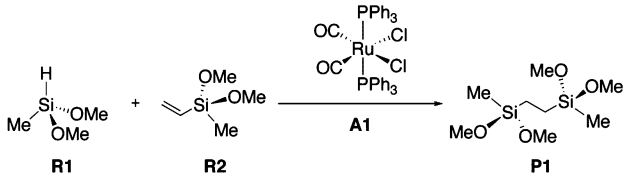

Scheme 2. Chalk−Harrod and Modified Chalk−Harrod Catalytic Cycles

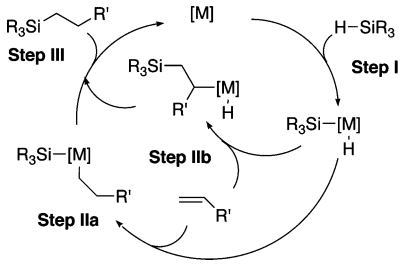

Harrod[18] (CH) and modified Chalk−Harrod[16,19−23] (mCH) catalytic cycles.[8,13,14,17,24−28] Both mechanisms involve an initial oxidative addition of a SiH-functional silane (e.g., **R1**) to the transition metal, M (step I, Scheme 2). In the CH mechanism, this is followed by a subsequent insertion of a C═C functional substrate (e.g., **R2**) into the M−H bond (step IIa), whereas in the mCH mechanism the C═C bond is inserted into the M−Si bond (step IIb). The final step (step III) for both mechanisms is the reductive elimination of the hydrosilylation product (e.g., **P1**).

More recently, alternative mechanisms have been proposed. These include the Glaser−Tilley mechanism[10,11] and a σ-bond metathesis (SBM) mechanism.[29,30] The latter is well established for early transition metal catalysts[31−35] and has recently also been considered in the realm of late transition metal catalysis.[36−46] The nature of our reactants excludes a Glaser−Tilley type mechanism; thus we concentrate only on the CH, mCH, and SBM mechanisms in this report.

Experimental Section

General Considerations. The silanes diethoxymethylvinylsilane and diethoxymethylsilane were purchased from GELEST and used as received. The ruthenium catalyst $RuCl_2(CO)_2(PPh_3)_2$ was purchased from STREM. ^{1}H and ^{29}Si NMR spectra were recorded at room temperature on a Bruker Avance 300 spectrometer in $CDCl_3$ or C_6D_6. All chemical shifts are in ppm referenced to the residual proton solvent resonance at δ 7.24 and 7.15 ppm, respectively (^{1}H) or to the external standard TMS (^{29}Si). Routine GC analysis was performed with an Agilent 6890 N gas chromatograph equipped with an RtX-200 column (Restek GmbH). Calibration was performed with pure samples of diethoxymethylvinylsilane, diethoxymethylsilane, and triethoxymethylsilane (purchased from GELEST) as well as bis(diethoxymethylsilyl)ethane and bis(diethoxymethylsilyl)ethene, which were independently prepared by literature methods.[47,48] For diethoxymethylethylsilane an response factor identical to that for diethoxymethylvinylsilane was assumed. GC-MS spectra were measured on an Agilent 6890/MSD 5973 GC/mass spectrometer at 70 eV.

Catalytic Run. A 25 mL two-necked round-bottomed flask equipped with a reflux condenser, argon inlet, and a magnetic stirring bar was charged under argon with 38 mg (50.5 μmol) of $RuCl_2(CO)_2(PPh_3)_2$. A 1.74 g (10.9 mmol) amount of $Me(Vi)Si(OEt)_2$ and 1.46 g (10.9 mmol) of $Me(H)Si(OEt)_2$ were added by syringe. The mixture was stirred and heated at 100 °C for 6 h. After cooling to room temperature, the reaction mixture was analyzed by GC and GC/MS.

The crude mixture was purified by distillation, leaving a mixture of $(EtO)_2MeSi-CH_2CH_2-SiMe(OEt)_2$ and (*E*)-$(EtO)_2MeSi-CH═CH-SiMe(OEt)_2$ in a combined yield of 1.91 g in a ratio of 86:14 (determined by the ^{1}H NMR integral of the CH_2CH_2 signal at 0.54 ppm vs the integral of the CH═CH signal at 6.64 ppm in $CDCl_3$). The ^{1}H NMR data of $(EtO)_2MeSi-CH_2CH_2-SiMe(OEt)_2$ and (*E*)-$(EtO)_2MeSi-CH═CH-SiMe(OEt)_2$ compare well with the literature values.[48,49]

$(EtO)_2MeSi-CH_2CH_2-SiMe(OEt)_2$: ^{1}H NMR (300.1 MHz, $CDCl_3$) δ 3.72 (q, 8 H, J = 7.0 Hz, H_2CO), 1.17 (t, 12 H, J = 7.0 Hz, H_3CCH_2), 0.54 (s, 4 H, CH_2CH_2), 0.07 (s, 6 H, H_3CSi); ^{29}Si NMR (59.6 MHz, $CDCl_3$) δ −4.42 (s); GC/MS *m*/*z* (relative abundance) 279 (4%, M − CH_3).

(*E*)-$(EtO)_2MeSi-CH═CH-SiMe(OEt)_2$: ^{1}H NMR (300.1 MHz, $CDCl_3$) δ 6.64 (s, 2 H, CH═CH), 3.75 (q, 8 H, J = 7.0 Hz, H_2CO), 1.18 (t, 12 H, J = 7.0 Hz, H_3CCH_2), 0.08 (s, 6 H, H_3CSi);

(18) Chalk, A. J.; Harrod, J. F. *J. Am. Chem. Soc.* **1965**, *87*, 16.
(19) Fernandez, M. J.; Esteruelas, M. A.; Jimenez, M. S.; Oro, L. A. *Organometallics* **1986**, *5*, 1519.
(20) Onopchenko, A.; Sabourin, E. T.; Beach, D. L. *J. Org. Chem.* **1983**, *48*, 5101.
(21) Randolph, C. L.; Wrighton, M. S. *J. Am. Chem. Soc.* **1986**, *108*, 3366.
(22) Schröder, M. A.; Wrighton, M. S. *J. Organomet. Chem.* **1977**, *128*, 345.
(23) Seitz, F.; Wrighton, M. S. *Angew. Chem., Int. Ed. Engl.* **1988**, *27*, 289.
(24) Sakaki, S.; Mizoe, N.; Musashi, Y.; Sugimoto, M. *J. Mol. Struct. (THEOCHEM)* **1999**, *462*, 533.
(25) Sakaki, S.; Mizoe, N.; Sugimoto, M. *Organometallics* **1998**, *17*, 2510.
(26) Sakaki, S.; Mizoe, N.; Sugimoto, M.; Musashi, Y. *Coord. Chem. Rev.* **1999**, *192*, 933.
(27) Sakaki, S.; Ogawa, M.; Musashi, Y.; Arai, T. *J. Am. Chem. Soc.* **1994**, *116*, 7258.
(28) Sakaki, S.; Sumimoto, M.; Fukuhara, M.; Sugimoto, M.; Fujimoto, H.; Matsuzaki, S. *Organometallics* **2002**, *21*, 3788.
(29) Crabtree, R. H. *Chem. Rev.* **1995**, *95*, 987.
(30) Arndtsen, B. A.; Bergman, R. G.; Mobley, T. A.; Peterson, T. H. *Acc. Chem. Res.* **1995**, *28*, 154.
(31) Fu, P. F.; Brard, L.; Li, Y. W.; Marks, T. J. *J. Am. Chem. Soc.* **1995**, *117*, 7157.
(32) Kesti, M. R.; Waymouth, R. M. *Organometallics* **1992**, *11*, 1095.
(33) Radu, N. S.; Tilley, T. D. *J. Am. Chem. Soc.* **1995**, *117*, 5863.
(34) Voskoboynikov, A. Z.; Parshina, I. N.; Shestakova, A. K.; Butin, K. P.; Beletskaya, I. P.; Kuzmina, L. G.; Howard, J. A. K. *Organometallics* **1997**, *16*, 4041.
(35) Woo, H. G.; Walzer, J. F.; Tilley, T. D. *J. Am. Chem. Soc.* **1992**, *114*, 7047.
(36) Hartwig, J. F.; Bhandari, S.; Rablen, P. R. *J. Am. Chem. Soc.* **1994**, *116*, 1839.
(37) Hutschka, F.; Dedieu, A.; Eichberger, M.; Fornika, R.; Leitner, W. *J. Am. Chem. Soc.* **1997**, *119*, 4432.
(38) Iverson, C. N.; Smith, M. R. *J. Am. Chem. Soc.* **1995**, *117*, 4403.
(39) Lee, J. C.; Peris, E.; Rheingold, A. L.; Crabtree, R. H. *J. Am. Chem. Soc.* **1994**, *116*, 11014.
(40) Luo, X. L.; Crabtree, R. H. *J. Am. Chem. Soc.* **1989**, *111*, 2527.
(41) Marder, T. B.; Norman, N. C.; Rice, C. R.; Robins, E. G. *Chem. Commun.* **1997**, 53.
(42) Maseras, F.; Duran, M.; Lledos, A.; Bertran, J. *J. Am. Chem. Soc.* **1992**, *114*, 2922.
(43) Milet, A.; Dedieu, A.; Kapteijn, G.; van Koten, G. *Inorg. Chem.* **1997**, *36*, 3223.
(44) Musaev, D. G.; Mebel, A. M.; Morokuma, K. *J. Am. Chem. Soc.* **1994**, *116*, 10693.
(45) Siegbahn, P. E. M.; Crabtree, R. H. *J. Am. Chem. Soc.* **1996**, *118*, 4442.
(46) Su, M. D.; Chu, S. Y. *J. Am. Chem. Soc.* **1997**, *119*, 5373.
(47) Lakhtin, V. G.; Nosova, V. M.; Kisin, A. V.; Ivanov, P. V.; Chernyshev, E. A. *Russ. J. Gen. Chem.* **2001**, *71*, 1252.
(48) Marciniec, B.; Maciejewski, H.; Gulinski, J.; Rzejak, L. *J. Organomet. Chem.* **1989**, *362*, 273.
(49) Watanabe, H.; Asami, M.; Nagai, Y. *J. Organomet. Chem.* **1980**, *195*, 363.

^{29}Si NMR (59.6 MHz, $CDCl_3$) δ −20.08 (s); ^{1}H NMR (300.1 MHz, C_6D_6) δ 6.98 (s, 2 H, CH═CH), 3.71 (q, 8 H, J = 7.0 Hz, H_2CO), 1.14 (t, 12 H, J = 7.0 Hz, H_3CCH_2), 0.22 (s, 6 H, H_3CSi); GC-MS *m*/*z* (relative abundance) 277 (47%, M − CH_3).

Reaction Products. The hydrosilylation of diethoxymethylvinylsilane with diethoxymethylsilane was performed at 100 °C for 6 h in the presence of $RuCl_2(CO)_2(PPh_3)_2$ (0.005 equiv) without solvent. After this reaction time, the conversion of the reactants is not fully complete and the formation of the hydrosilylation product, $(EtO)_2MeSi-CH_2CH_2-SiMe(OEt)_2$ (54%), is accompanied by several side reactions, including dehydrogenative silylation resulting in the formation of (*E*)-$(EtO)_2MeSi-CH=CH-SiMe(OEt)_2$[48] (9%) and diethoxymethylethylsilane (6%) formed by the hydrogenation of the vinylsilane.[50] Another byproduct is triethoxymethylsilane (6%), presumably formed by a H/OEt exchange reaction of diethoxymethylsilane. The formation of the reaction products was successfully confirmed by NMR spectroscopy and GC-mass spectrometry. The product distribution also contains 17% of unreacted starting materials ($Me(Vi)Si(OEt)_2$, 9%; $Me(H)Si(OEt)_2$, 8%) and 8% of unidentified compounds. The hydrosilylation product is the major component of the product mixture. Our computational study addresses the mechanism of its formation.

Computational Methods

Density functional theory[51,52] (DFT) was employed for the calculation of all reactants, transition states (TSs), intermediates, and products. In all calculations, the ruthenium atom was described by a small-core, quasi-relativistic, effective core potential with the associated (7s6p5d)/[5s3p3d] valence basis set,[53] while the 6-31G-(d,p) basis set[54−56] was used for all other atoms. Initial geometry optimizations of the minima along the reaction path were performed with the gradient-corrected BP86 functional,[57−59] in order to take advantage of the resolution-of-the-identity(RI)-DFT approach,[60] as implemented in TURBOMOLE.[61−64] All structures were subsequently refined in Gaussian03,[65] by carrying out geometry optimizations with the B3LYP hybrid functional,[57,59,66−69] which has been shown to produce reliable thermochemical data for ruthenium-based compounds.[70−72]

Scheme 3. Uncatalyzed Hydrosilylation Reaction between R1 and R2

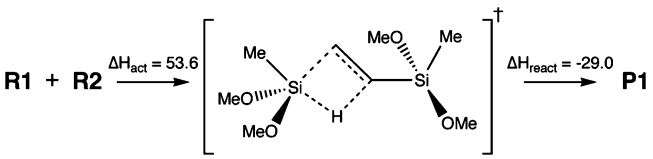

Gaussian03 was employed in the refinement process as the search for TSs often made use of the synchronous transit-guided quasi-Newton method,[73,74] available in this package. Frequency calculations were performed on all optimized structures, using the B3LYP functional, to characterize the stationary points as minima or TSs, as well as for the calculation of zero-point energies (ZPE), enthalpies (*H*), entropies (*S*), and Gibbs free enthalpies (*G*) at 298 K.

Results and Discussion

The uncatalyzed hydrosilylation reaction involves the addition of **R1** to **R2** in a concerted mechanism (Scheme 3). The transition state contains a four-membered ring with the H-abstraction from **R1** and the Si−C bond formation occurring concomitantly. The reaction is strongly exothermic (ΔH_{react} = −29.0 kcal/mol); however, the activation enthalpy (ΔH_{act} = 53.6 kcal/mol) is prohibitively high, and thus a catalyst is needed to lower the activation enthalpy for the hydrosilylation to an operational level (i.e., <25 kcal/mol).

The Catalyst. The octahedral complex **A1** has five positional stereoisomers; each of these was optimized in order to determine the most favorable arrangement for the hexacoordinated ruthenium. The three isomers with the triphenylphosphine (PPh_3) ligands in the *cis* position are all strongly destabilized relative to the two *trans*-PPh_3 isomers, due to steric repulsion, and they were therefore not investigated further. X-ray structures are available only for the two isomers with the *trans* arrangement of the PPh_3 ligands.[75,76] These crystal structures provide a good test for the accuracy of the computed geometries. The optimized structure of the *cis*-dicarbonyl-*cis*-dichloro-*trans*-bis(triphenylphosphine) (cct) isomer is very similar to the crystal structure of this compound, [75] with a root-mean-square deviation (rmsd) for the heavy atom coordinates of 0.38 Å (Figure 1a); if only the atoms within the first coordination sphere are considered, the agreement with experiment is slightly improved, with the rmsd decreasing to 0.31 Å. However, for the ttt isomer the positioning of the phenyl substituents differs between the experimental[76] and optimized structures. The rmsd for the heavy atom coordinates of these structures (Figure 1b) is 5.57 Å as a result of the different twist of the PPh_3 substituents (possibly due to crystal-packing effects); if we again consider only those atoms directly coordinated to the metal center, the rmsd value is very small (0.13 Å). The DFT calculations correctly reproduce the changes in bond lengths that one would expect as a result of the stronger *trans* influence of the carbon monoxide relative to the chloride ligand. For example, the Ru−C(O) bond length increases from 1.88 Å (1.86 Å exptl) in the cct complex to 1.95 Å (1.95, 2.06 Å exptl) in the ttt complex.

(50) Product distribution determined by GC analysis of the crude reaction mixture (see Experimental Section).

(51) Kohn, W.; Sham, L. J. *Phys. Rev.* **1965**, *140*, 1133.
(52) Parr, R. G.; Yang, W. T. *Density Functional Theory of Atoms and Molecules*; Oxford University Press: New York, 1989.
(53) Andrae, D.; Häussermann, U.; Dolg, M.; Stoll, H.; Preuss, H. *Theor. Chim. Acta* **1990**, *77*, 123.
(54) Hariharan, P. C.; Pople, J. A. *Theor. Chim. Acta* **1973**, *28*, 213.
(55) Hehre, W. J.; Ditchfield, R.; Pople, J. A. *J. Chem. Phys.* **1972**, *56*, 2257.
(56) Ditchfield, R.; Hehre, W. J.; Pople, J. A. *J. Chem. Phys.* **1971**, *54*, 724.
(57) Becke, A. D. *Phys. Rev. A* **1988**, *38*, 3098.
(58) Perdew, J. P. *Phys. Rev. B* **1986**, *33*, 8822.
(59) Vosko, S. H.; Wilk, L.; Nusair, M. *Can. J. Phys.* **1980**, *58*, 1200.
(60) Eichkorn, K.; Treutler, O.; Ohm, H.; Häser, M.; Ahlrichs, R. *Chem. Phys. Lett.* **1995**, *240*, 283.
(61) *TURBOMOLE*, V. 5.7.1; COSMOlogic G.m.b.H. & Co. KG; Leverkusen, Germany, 2004.
(62) Ahlrichs, R.; Bär, M.; Häser, M.; Horn, H.; Kölmel, C. *Chem. Phys. Lett.* **1989**, *162*, 165.
(63) Eichkorn, K.; Treutler, O.; Ohm, H.; Häser, M.; Ahlrichs, R. *Chem. Phys. Lett.* **1995**, *242*, 652.
(64) Treutler, O.; Ahlrichs, R. *J. Chem. Phys.* **1995**, *102*, 346.
(65) Frisch, M. J.; et. al. *Gaussian 03*, V. C.01; Gaussian, Inc.; Wallingford, CT, 2004.
(66) Becke, A. D. *J. Chem. Phys.* **1993**, *98*, 5648.
(67) Lee, C. T.; Yang, W. T.; Parr, R. G. *Phys. Rev. B* **1988**, *37*, 785.
(68) Stephens, P. J.; Devlin, F. J.; Chabalowski, C. F.; Frisch, M. J. *J. Phys. Chem.* **1994**, *98*, 11623.
(69) Hertwig, R. H.; Koch, W. *Chem. Phys. Lett.* **1997**, *268*, 345.
(70) Baker, J.; Muir, M.; Andzelm, J.; Scheiner, A. In *Chemical Applications of Density-Functional Theory*; ACS Symp. Ser. 629; American Chemical Society: Washington, DC, 1996; p 342.
(71) Niu, S. Q.; Hall, M. B. *Chem. Rev.* **2000**, *100*, 353.
(72) Vyboishchikov, S. E.; Bühl, M.; Thiel, W. *Chem. Eur. J.* **2002**, *8*, 3962.
(73) Peng, C. Y.; Ayala, P. Y.; Schlegel, H. B.; Frisch, M. J. *J. Comput. Chem.* **1996**, *17*, 49.
(74) Peng, C. Y.; Schlegel, H. B. *Isr. J. Chem.* **1993**, *33*, 449.
(75) Batista, A. A.; Zukermanschpector, J.; Porcu, O. M.; Queiroz, S. L.; Araujo, M. P.; Oliva, G.; Souza, D. H. F. *Polyhedron* **1994**, *13*, 689.
(76) De Araujo, M. P.; Porcu, O. M.; Batista, A. A.; Oliva, G.; Souza, D. H. F.; Bonfadini, M.; Nascimento, O. R. *J. Coord. Chem.* **2001**, *54*, 81.

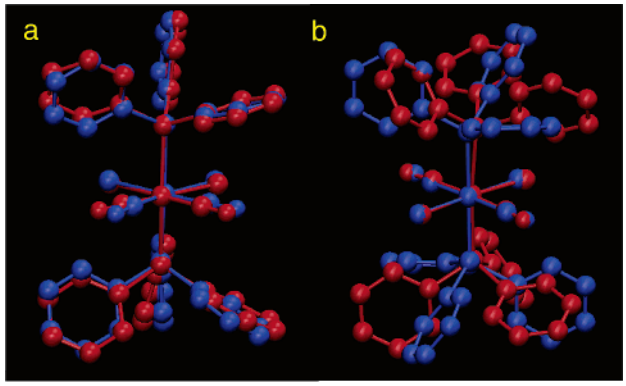

Figure 1. Superposition of optimized (red) and X-ray (blue) structures of **A1**: (a) cct isomer, (b) ttt isomer.

Experimental vibrational frequencies are available[75] for the C−O and Ru−Cl stretching modes of the cct isomer. The C−O stretching wavenumbers are 2060 and 1998 cm^{-1}, which compare well to the calculated values of 2115 (symmetric stretch) and 2061 (antisymmetric stretch) cm^{-1}. Similarly the calculated Ru−Cl stretching wavenumbers (268 (as) and 295 (s) cm^{-1}) are within 5% of the experimental values (278 and 302 cm^{-1}, respectively). We consider the overall agreement between the available experimental and theoretical data for **A1** as satisfactory and as a validation of the chosen DFT methodology for the current study.

Both the cct and ttt configurations are minima on the potential energy surface, but the cct isomer (Figure 1a) is 14.4 kcal/mol more stable than ttt. This can easily be understood in a "pull−push" scenario, where the strong π-accepting (pull) nature of the carbonyl ligands is complemented by the *trans* arrangement with the π-donating (push) chloride ligands. We have confirmed that subsequent intermediates and products in the catalytic cycle of the ttt isomer are also significantly destabilized relative to those of the cct isomer. Thus, in the remainder of this paper, we shall only consider reactions starting from the cct isomer (**A1**) as depicted in Scheme 1.

Scheme 4. Possible Variants of A1 Resulting from the Induction Phase

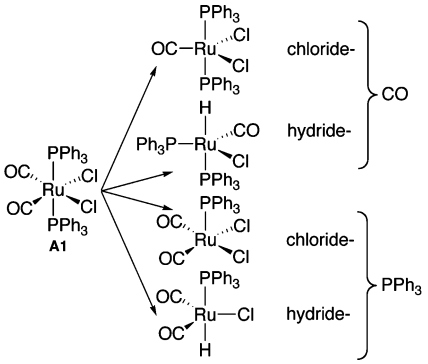

Chalk−Harrod Mechanism, Overview. In order for **A1** to become active in the CH or mCH mechanism, two ligands need to be removed from the metal to generate a formally tetracoordinated ruthenium(II) complex. The nature of the catalyst formed in this induction period is unknown; therefore we consider two possible starting points, the initial decoordination of either a CO ligand (resulting in the CO path) or a PPh_3 ligand (resulting in the PPh_3 path). The direct dissociation of a chloride ligand was disregarded due to the large endothermicity expected for this process in the absence of a polar solvent. However, we have considered the exchange of a chloride ligand with a hydride ligand, as explained below, during the induction period. Hence, there are four possible paths arising from the induction period (Scheme 4).

In principle, each of the active complexes may follow the CH or mCH mechanism, but the latter can be excluded by considering the relative enthalpy ($\Delta H(298)$) of the CH and mCH intermediates, the compounds resulting from step IIa and step IIb, respectively (Scheme 2). For the chloride−CO path,

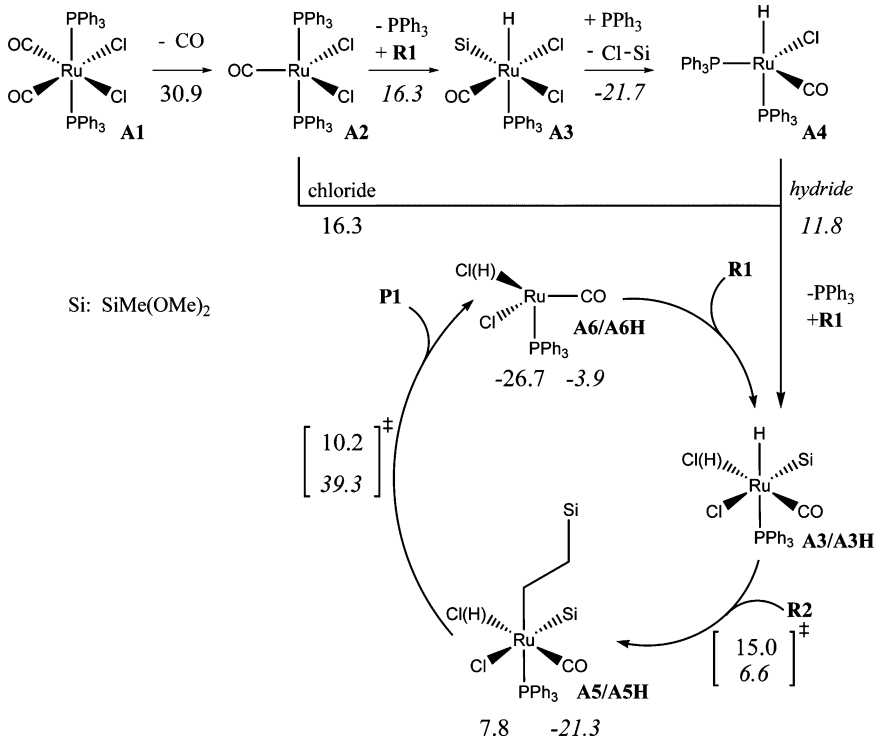

Figure 2. CO paths and the associated induction mechanism. Relative enthalpies are reported in kcal/mol. Values in italics correspond to the hydride mechanism.

Table 1. Reaction Enthalpies of the CH Mechanisms for A1[a]

reaction, CO paths	$\Delta H(298)$	reaction, PPh_3 paths	$\Delta H(298)$
		Chloride Mechanisms	
A1 → **A2** + CO	30.9	**A1** → **A7** + PPh_3	15.4
A2 + **R1** → **A3** + PPh_3	16.3	**A7** + **R1** → **A9** + PPh_3	13.3
A3 + **R2** → **TS(A3-A5)**	15.0	**A9** + **R2** → **TS(A9−A10)**	6.1
A3 + **R2** → **A5**	7.8	**A9** + **R2** → **A10**	−0.6
A5 → **TS(A5−A6)**	10.2	**A10** → **TS(A10−A11)**	9.0
A5 → **A6** + **P1**	−26.7	**A10** → **A11** + **P1**	−14.7
		Hydride Mechanisms	
A3 + PPh_3 → **A4** + Cl−Si	−21.7	**A7** + **R1** → **TS(A7−A8)**	1.9
A4 + **R1** → **A3H** + PPh_3	11.8	**A7** + **R1** → **A8** + Cl−Si	−11.9
A3H + **R2** → **TS(A3H−A5H)**	6.6	**A8** + **R1** → **A9H** + PPh_3	9.0
A3H + **R2** → **A5H**	−21.3	**A9H** + **R2** → **TS(A9H−A10H)**	6.7
A5H → **TS(A5H−A6H)**	39.3	**A9H** + **R2** → **A10H**	−12.0
A5H → **A6H** + **P1**	−3.9	**A10H** → TS(A10H−**A11H**)	23.4
		A10H → **A11H** + **P1**	11.0

[a] Relative enthalpies are calculated from the data provided in Table S1 of the Supporting Information. All values are given in kcal/mol. Refer to Figures 2 and 3 for notation.

the CH intermediate is 32.2 kcal/mol more stable than the mCH intermediate, and within the hydride−CO path the CH intermediate is 10.8 kcal/mol more stable than the mCH intermediate. Similarly, on the chloride−PPh_3 path, the CH intermediate lies 11.2 kcal/mol below the mCH intermediate, and in the hydride−PPh_3 path no intermediate for the mCH mechanism could be located. Hence, the CH intermediates (insertion into a Ru−H bond) are generally favored over the mCH intermediates (insertion into a Ru−Si bond) by a large margin. Therefore, we decided to compute the transition states only for the CH pathways.

Chalk−Harrod Mechanism, CO Paths. After the initial dissociation of the carbonyl ligand (Figure 2, **A1** → **A2**), the entry point to the catalytic cycle may be reached either directly (**A3**, chloride path) or after replacement of a chloride ligand by a hydride ligand (**A3H**, hydride path). The first step in the induction mechanism (dissociation of CO) is a barrierless, uphill process, which is endothermic by 30.9 kcal/mol (Table 1). In the chloride mechanism, the subsequent dissociation of PPh_3 with concomitant oxidative addition of **R1** requires another 16.3 kcal/mol. Hence, the initial entry into the catalytic cycle (formation of **A3**) results in a destabilization of 47.2 kcal/mol, relative to **A1**.

The alternative hydride mechanism involves the substitution of a chloride ligand by a hydride ligand after the initial oxidative addition. This transformation yields a five-coordinate species (**A4**) that is analogous to the chloride complex **A2**, although 5.4 kcal/mol more stable (Figure 2). The subsequent dissociation of PPh_3 and oxidative addition of **R1** requires 11.8 kcal/mol, such that **A3H** lies 37.3 kcal/mol above **A1** and the separated reactants and products. Thus, during the induction period, the formation of **A3H** should be preferred over that of **A3**.

Within the catalytic cycle, the insertion of **R2** into the Ru−H bond was calculated for both hydride and chloride variants, and the barrier to insertion was found to be 8.4 kcal/mol lower in the case of the hydride (ΔH_{act}(**A3H**) = 6.6 kcal/mol, Table 1). Similarly, the CH intermediate for the hydride path, **A5H**, is produced in a strongly exothermic reaction (ΔH_{react}(**A5H**) = −21.3 kcal/mol), while the formation of **A5** is mildly endothermic (ΔH_{react}(**A5**) = 7.8 kcal/mol). However, the final reductive elimination step favors the chloride mechanism, with a barrier of 10.2 kcal/mol, compared to the hydride path, which requires a large activation enthalpy of 39.3 kcal/mol for the formation of the product.

On the basis of these results, we can exclude the CO paths as mechanistic possibilities for **A1**: the induction is much too endothermic overall (47.2 and 37.3 kcal/mol for the chloride and hydride variants, respectively) and product formation has a large barrier of 39.3 kcal/mol in the hydride case.

Chalk−Harrod Mechanism, PPh_3 Path. The main difference from the CO path arises in the induction period. The initial dissociation of PPh_3 (**A1** → **A7**, Figure 3) is much more favorable than the CO dissociation, resulting in an enthalpy increase of only 15.4 kcal/mol (Table 1). In order for the chloride path to be active, the second PPh_3 ligand also needs to dissociate. As before, this second dissociation is expected to occur simultaneously with the oxidative addition of **R1**. This oxidative addition favors a reorientation of the CO ligands, with the resulting Ru(IV) complex (**A9**) being more stable when the CO ligands occupy *trans* positions. Despite the ease of dissociating the first PPh_3 ligand, there is a large enthalpic penalty (38.9 kcal/mol) for the removal of the second PPh_3 ligand. However, the oxidative addition partially compensates this loss, such that **A9** is destabilized by 28.7 kcal/mol, relative to **A1**. The barrier to the insertion of **R2** to form the CH intermediate **A10** is low (6.1 kcal/mol), and the intermediate is formed in a thermoneutral reaction (ΔH_{react}(**A10**) = −0.6 kcal/mol). Unlike the chloride−CO path, the reductive elimination resulting in **P1** is now the rate-determining step within the catalytic cycle,

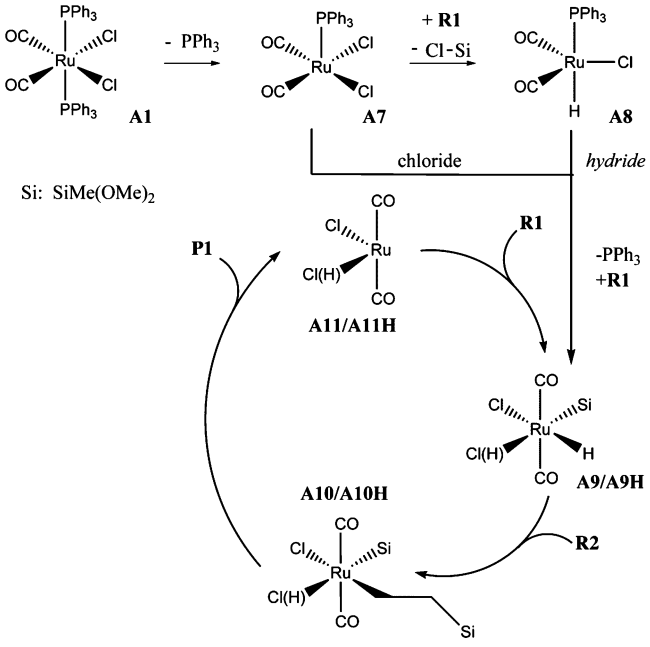

Figure 3. PPh_3 paths and the associated induction mechanism.

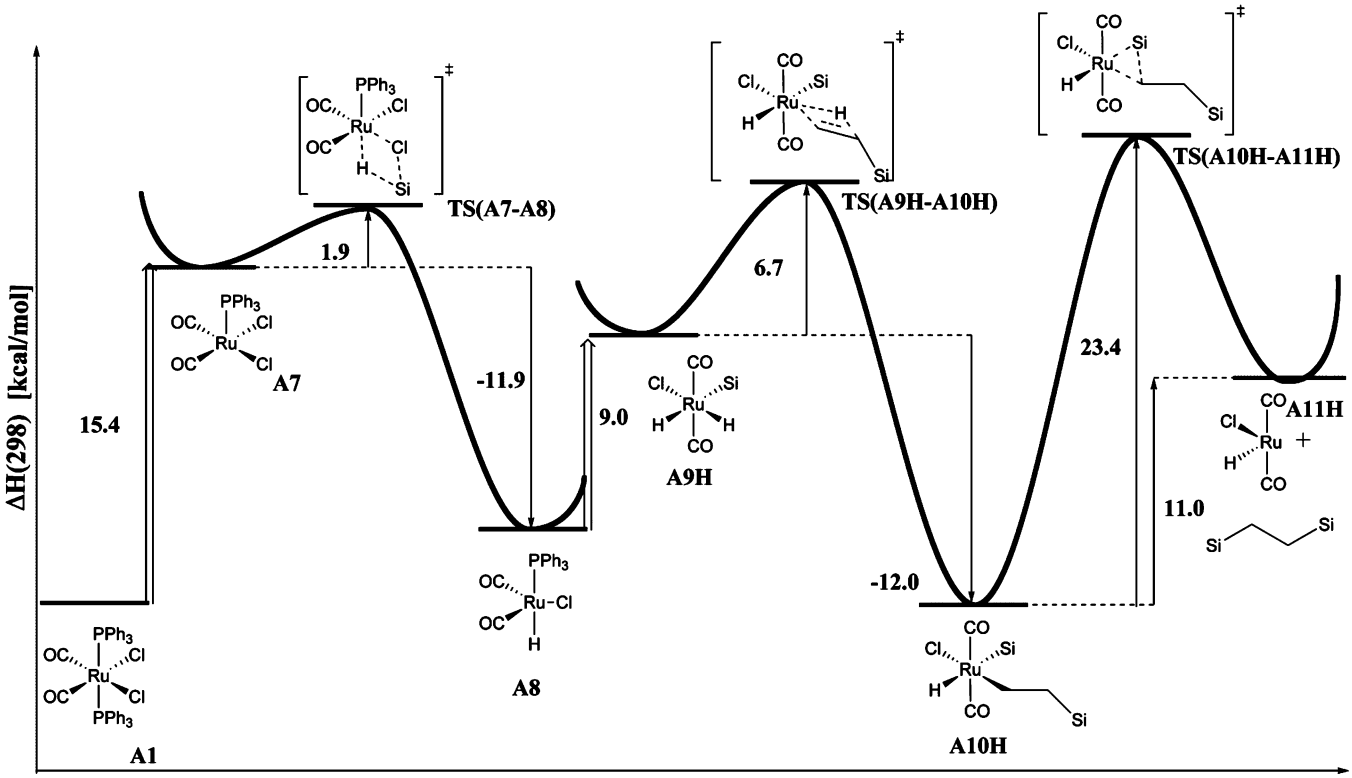

Figure 4. Enthalpy profile of the hydride−PPh_3 mechanism. Relative enthalpies in kcal/mol.

although the barrier (ΔH_{act}(**A10**) = 9.0 kcal/mol) is still modest. The product is formed in an exothermic reaction (ΔH_{react}(**A11**) = −14.7 kcal/mol).

The hydride−PPh_3 path is generated by passing through the intermediate structure **A8**, which is formed through a SBM reaction, in which the Si−H bond of **R1** is replaced by the Si−Cl bond, and the Ru−Cl bond by the Ru−H bond (**TS(A7−A8)**, Figure 4). The SBM ligand exchange at the Ru atom is facile, with an activation barrier of only 1.9 kcal/mol. The dissociation of chlorodimethoxymethylsilane (Cl−Si) produces the hydride ruthenium(II) complex in an exothermic reaction (ΔH_{react}(**A8**) = −11.9 kcal/mol).

Entry into the catalytic cycle occurs after a subsequent dissociation of the second PPh_3 ligand and the concomitant oxidative addition of **R1**, yielding **A9H**. Similar to the chloride path, the dissociation of the second PPh_3 ligand is strongly destabilizing (ΔH = 37.1 kcal/mol), although the oxidative addition of **R1** partially compensates such that the reaction (**A8** → **A9H**) is endothermic by 9.0 kcal/mol. Qualitatively, the catalytic cycle of the hydride−PPh_3 path is analogous to the hydride−CO path; while the insertion of **R2** to form **A10H** needs little activation enthalpy (ΔH_{act}(**A9H**) = 6.7 kcal/mol) and the formation of the intermediate is exothermic, the subsequent step—the generation of the product—requires the surmounting of a larger barrier (ΔH_{act}(**A10H**) = 23.4 kcal/mol), and the reaction is endothermic by 11.0 kcal/mol.

The difference in the reaction energies for the hydride and the chloride mechanisms of the PPh_3 paths is quite pronounced, since the product formation is endothermic in the former case and exothermic in the latter. This difference is reflected in the geometry of the corresponding TSs (Figure 5). In the chloride mechanism **TS(A10−A11)** (Figure 5a) is structurally closer to its reactants, while in the hydride mechanism, **TS(A10H−A11H)** (Figure 5b) is closer in structure to its products. The forming Si−C bond in the chloride mechanism is still relatively weak in the TS at 2.04 Å. Conversely, in the hydride mechanism, the Si−C bond is relatively short (1.98 Å) and the Ru−Si bond is essentially broken (3.10 Å). The relative similarity between the structure of the TS and the reactants (chloride) or products (hydride) is consistent with the Hammond postulate.[77]

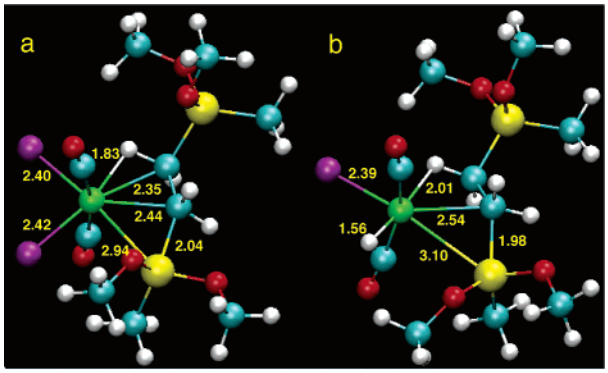

Figure 5. Transition states in the product formation step of the PPh_3 paths: (a) **TS(A10−A11)**; (b) **TS(A10H−A11H)**.

In summary, the hydride−PPh_3 path is favored over the chloride−PPh_3 path in the induction phase, because the entry point of the catalytic cycle is more accessible energetically with a small barrier for the SBM reaction **A7** → **A8**. In all cases examined thus far the barrier leading to the active species in the catalytic cycle (e.g., **A9H**) could not be located on the potential energy surface, as this reaction is expected to be quite complex. i.e., dissociation of a ligand with concomitant oxidative addition of a second ligand and (potentially) rearrangement in the coordination sphere. Given that in all cases this step was found to be endothermic (>9 kcal/mol), and the dissociation of the second PPh_3 ligand is strongly destabilizing (>37 kcal/mol), the barrier to this type of reaction is expected to be prohibitive. Therefore, we considered alternative mechanisms.

(77) Hammond, G. S. *J. Am. Chem. Soc.* **1955**, *77*, 334.

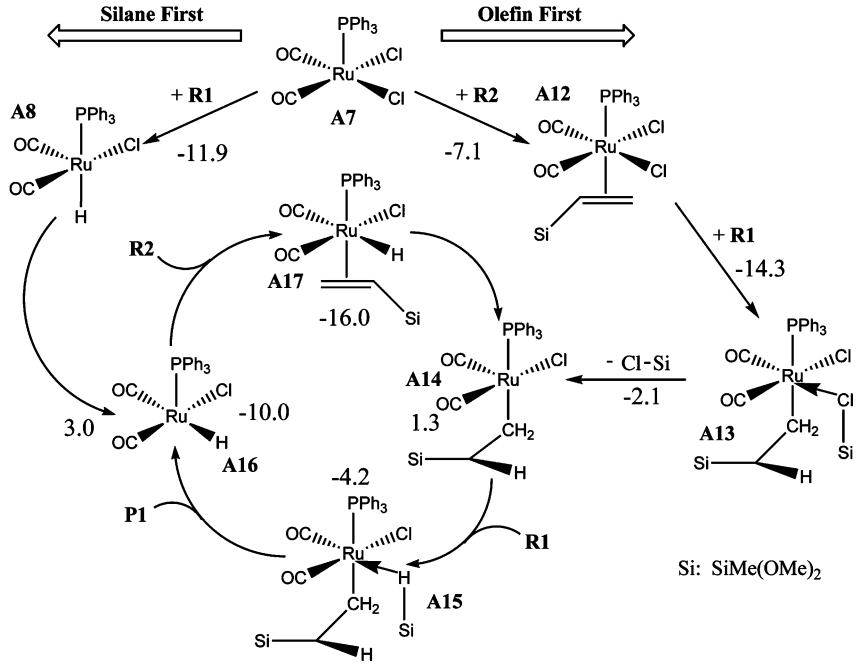

Figure 6. SBM catalytic cycle with two alternative induction mechanisms defined by the initial addition of either the silane (left) or the olefin (right). Reaction enthalpies in kcal/mol.

Table 2. Reaction Enthalpies of the SF and OF Induction Mechanisms and of the SBM Catalytic Cycle for A1[a]

SF induction mechanism	$\Delta H(298)$
A7 + **R1** → **TS(A7-A8)**	1.9
A7 + **R1** → **A8** + Cl−Si	−11.9
A8 → **TS(A8-A16)**	13.7
A8 → **A16**	3.0
OF induction mechanism	$\Delta H(298)$
A7 + **R2** → **A12**	−7.1
A12 + **R1** → **TS(A12-A13)**	32.1
A12 + **R1** → **A13**	−14.3
A13 → **A14** + Cl−Si	−2.1
SBM catalytic cycle	$\Delta H(298)$
A14 + **R1** → **A15**	−4.2
A15 → **TS(A15-A16)**	21.8
A15 → **A16** + **P1**	−10.0
A16 + **R2** → **A17**	−16.0
A17 → **TS(A17−A14)**	4.4
A17 → **A14**	1.3

[a] Relative energies and enthalpies are calculated from the data provided in Table S1 of the Supporting Information. All values are given in kcal/mol. Refer to Figures 6 and 8 for notation.

***σ*-Bond Metathesis Mechanism, Overview.** The investigation of the CH mechanisms has shown (1) the initial dissociation of a PPh_3 ligand is strongly favored over the dissociation of a CO ligand and (2) the SBM reaction resulting in the exchange of a hydride ligand with a chloride ligand provides a facile route to the hydride mechanism. We have incorporated these features into a new mechanism (Figure 6, left-hand side) and have additionally considered an alternative starting point, where the olefin (**R2**) coordinates directly to the metal center and the addition of **R1** occurs thereafter (Figure 6, right-hand side). The different induction mechanisms are distinguished by the addition of the "olefin-first" (OF) or the addition of the "silane-first" (SF).

***σ*-Bond Metathesis Mechanism, OF Path.** The initial dissociation of PPh_3 requires 15.4 kcal/mol; however, this is partially compensated for by the η^2-coordination of **R2** in an unhindered process, which lowers the enthalpy by 7.1 kcal/mol (Table 2). The addition of **R1** at this point in the mechanism

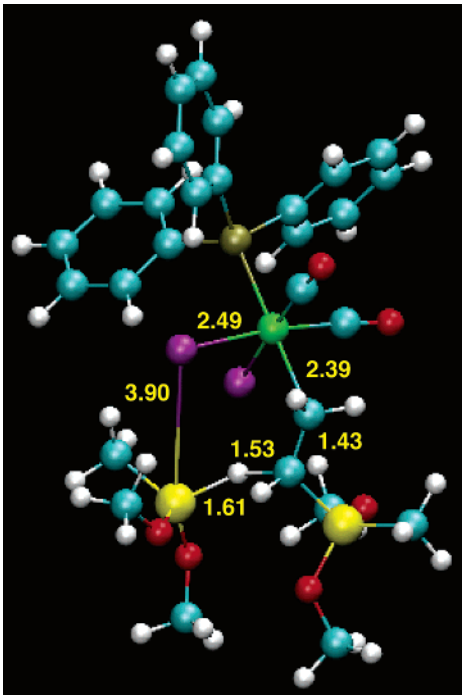

Figure 7. Transition state of the hydride formation step in the OF induction path. Distances in Å.

results in a concerted reaction, where the silane H atom is abstracted by the α-carbon atom (relative to the silicon) of **R2** and the Si atom of **R1** forms a bond with the neighboring chloride ligand to generate Cl−Si, which in turn is coordinated to the metal center through a dative bond (**TS(A12−A13)**, Figure 7). Despite its exothermicity (ΔH_{react}(**A13**) = −14.3 kcal/mol), this concerted process requires a large activation enthalpy of 32.1 kcal/mol. This is due primarily to the strain in the TS, as the active center contains a strongly distorted six-membered ring (Figure 7). Additionally, the attacking silane does not interact directly with the metal center (Ru- - -Si = 4.59 Å) during the SBM reaction and the Si−Cl *σ*-bond (3.90 Å) is not yet formed. Furthermore, the interaction between the metal

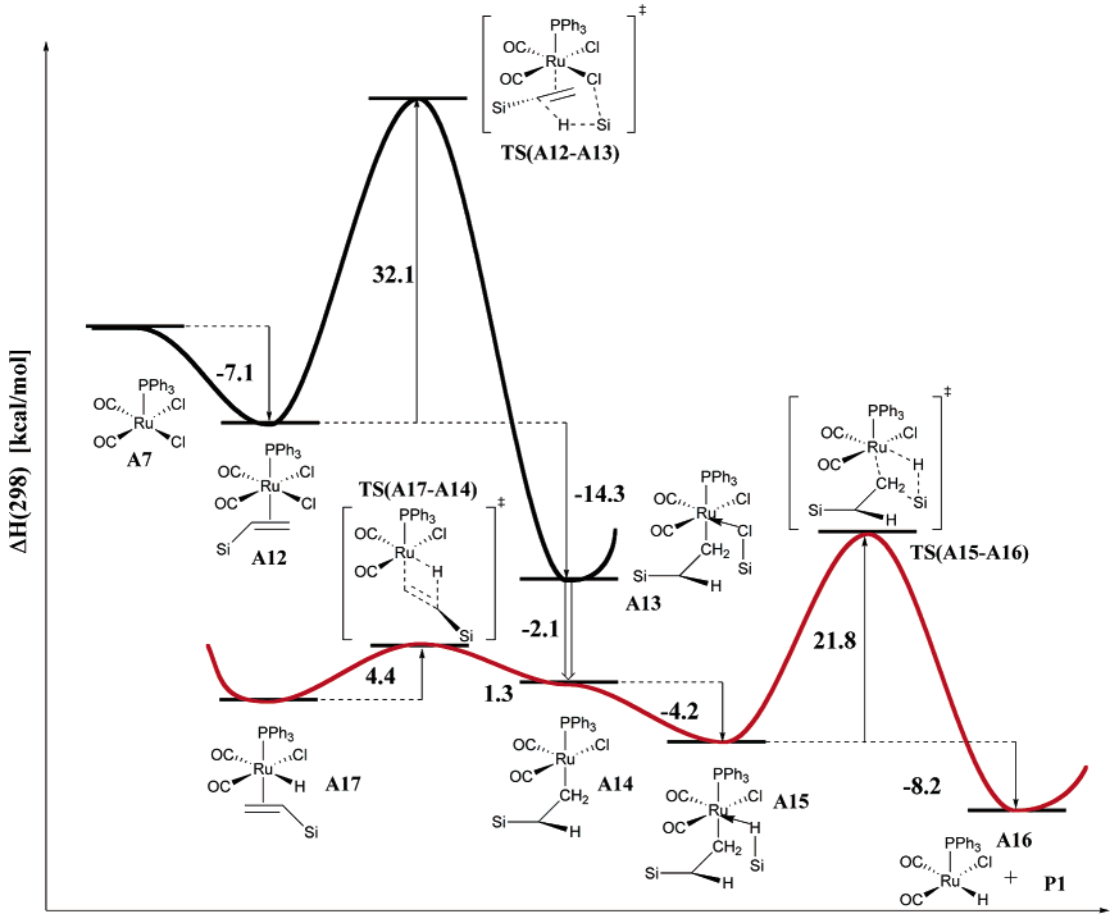

Figure 8. Enthalpy profile for the SBM mechanism. Relative enthalpies in kcal/mol. Red curve: catalytic cycle. Black curve: OF induction mechanism. The red curve is shifted downward for the sake of clarity.

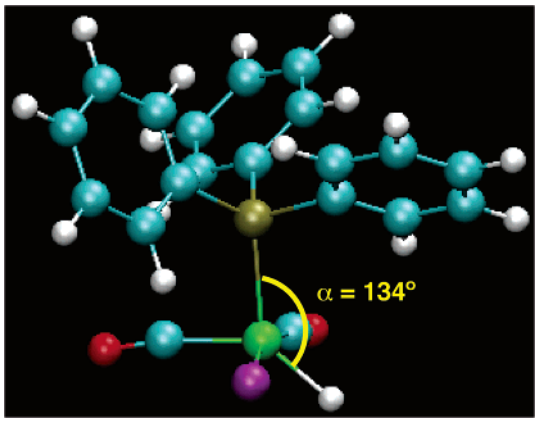

Figure 9. TS for the isomerization reaction of **A8** → **A16**.

center and the β-carbon atom of **R2** is also quite weak (2.39 Å). Thus, neither the C−C bond of **R2** nor the Si−H bond of **R1** has been activated by ruthenium, and as such, the catalyst has little effect in lowering the barrier.

From **A13**, the chlorosilane will dissociate to form **A14** in a mildly exothermic step, which is the entry point to the SBM catalytic cycle (red curve, Figure 8) for the OF induction path. The barrier to the dissociation of the Cl−Si in forming **A14** is expected to be negligible. A relaxed PES scan along the reaction coordinate of **A13** → **A14** indicates a maximum barrier of 1.6 kcal/mol (ΔE). However, a stationary point could not be located for the TS of this reaction, and as such, this barrier is not included in the enthalpy profile (Figure 8).

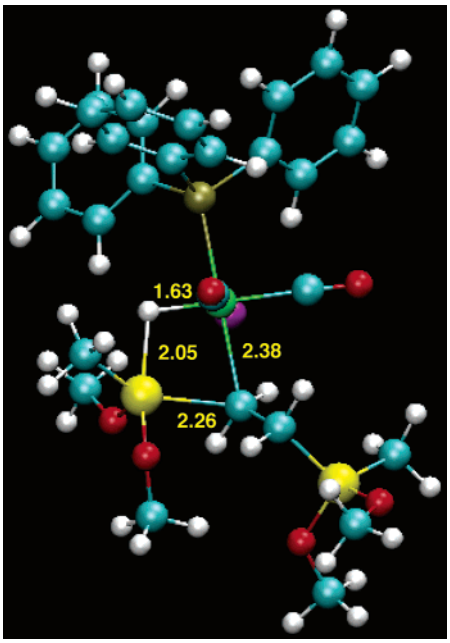

Figure 10. Transition state of the product formation step in the SBM catalytic cycle. Distances in Å.

***σ*-Bond Metathesis Mechanism, SF Path.** The large barrier calculated for the OF induction mechanism excludes this as a viable pathway to the SBM catalytic cycle. Thus, we returned to the induction mechanism described in the hydride−PPh_3 CH induction process (Figure 3). This mechanism leads to the exchange of a chloride ligand for a hydride ligand with a mini-

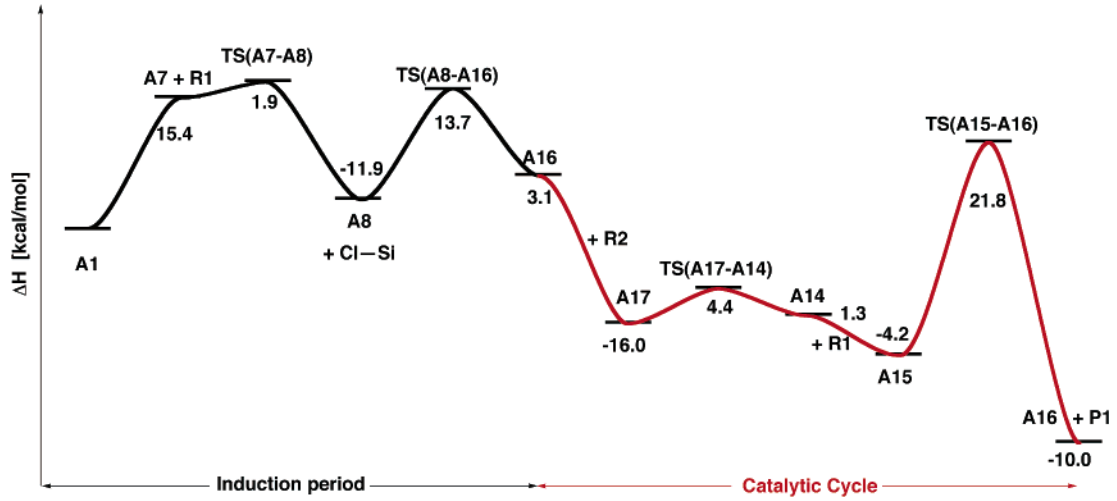

Figure 11. Relative enthalpy profile of the predicted mechanism for the hydrosilylation of **R2** by **R1** with the **A1** catalyst. Induction period in black; catalytic cycle in red. The numerical values given are barriers in the case of the TSs and reaction enthalpies relative to the preceding minimum otherwise (kcal/mol).

mal barrier (1.9 kcal/mol), in an exothermic SBM reaction forming the trigonal bipyramidal structure of **A8** (ΔH_{react}(**A8**) = −11.9 kcal/mol). The product of this reaction is an isomer of **A16** (square pyramidal structure), and the conversion between these two structures is possible through a repositioning of the hydride ligand. The P−Ru−H angle (α, Figure 9) in **A8** is 172.7°, while in **A16** α is decreased to 84.0°. The barrier to shifting the hydride ligand from an axial (**A8**) to an equatorial (**A16**) position is 13.7 kcal/mol. Thus, the initial formation of the hydride form of the catalyst (i.e., **A1** → **A8**) represents the rate-determining step in the activation barrier, while the isomerization reaction, relative to **A1**, proceeds more rapidly.

The calculated barrier to forming **A8** is significantly lower than the maximum barrier found in the OF induction pathway. Thus, the SF induction path is the preferred mechanism for **A1** to enter the SBM catalytic cycle.

***σ*-Bond Metathesis Mechanism.** The generation of **A16** in the SF induction path is followed by the coordination of **R2** into the vacant axial position, to form **A17**. This is an exothermic, barrierless reaction (ΔH_{react}(**A17**) = −16.0 kcal/mol), and the resulting η^2 complex (Figure 8) can easily abstract the hydride ligand (ΔH_{act}(**A17**) = 4.4 kcal/mol) to generate **A14** in a thermoneutral reaction (ΔH_{react}(**A14**) = 1.3 kcal/mol).

The dative coordination of the silane at the vacant coordination site of **A14** results in a decrease in the reaction enthalpy in a second unhindered process (ΔH_{react}(**A15**) = −4.2 kcal/mol, Table 2). The formation of the product and the regeneration of the active species (**A16**, Figure 8) will then occur through a third SBM reaction, whereby the H−Si bond is broken to form a bond between the hydride and ruthenium, while the silane forms a covalent bond with the carbon formerly bound to the metal center (Figure 10). The barrier to this reaction is consistent with the observed activity, at 21.8 kcal/mol, and is the rate-determining step in the catalytic cycle.

Figure 11 shows the complete enthalpy profile of the proposed reaction mechanism (i.e., SF induction followed by the SBM catalytic cycle).

Entropic Effects. Up to this point, we have considered only the enthalpies (ΔH) of reaction and activation. Of course, equilibria and reaction rates depend on the corresponding Gibbs free enthalpies ($\Delta G = \Delta H - T\Delta S$). We have computed the entropic contributions by applying the harmonic oscillator/rigid rotor approximation. The resulting ΔG values are listed in the Supporting Information, but they should be viewed with some caution, for two reasons. First, the computed entropic contributions refer to the gas phase and thus neglect solvation and desolvation effects in solution, which may be substantial. Second, the harmonic oscillator/rigid rotor approximation is known to be problematic in the case of weakly bound complexes (such as **A15**) due to the large number of low-energy vibrational modes, which in turn have large contributions to the entropy. Given this situation, the following discussion will not focus on the computed ΔG values, but rather on how the computed enthalpy profile (Figure 11) is qualitatively affected by the entropic contributions. The main such effect is that association reactions suffer from an entropic penalty because of the loss of translational and rotational degrees of freedom (typically around 10 kcal/mol at 298 K in the gas phase), while dissociation reactions are entropically favored in an analogous manner. In solution, these entropic effects will be less pronounced than in the gas phase due to solvation and desolvation, but they will be present to some extent.

Looking at the induction phase (Figure 11, black part), the initial dissociation of PPh_3 (**A1** → **A7**) becomes more facile on the ΔG scale because of the entropic contributions, but the subsequent association of **R1** in **TS(A7-A8)** becomes less facile for the same reason. Relative to **A1**, **TS(A7−A8)** is thus destabilized to a similar extent on the ΔH and ΔG scales (by 17.3 and 16.4 kcal/mol, respectively). The dissociation of Cl−Si in the formation of **A8** is favored from an entropic perspective (ΔH = 3.5 kcal/mol, ΔG = −14.0 kcal/mol, relative to **A1**). The following isomerization reaction (**A8** → **A16**) does not involve any association or dissociation, and as such, entropic effects play only a minor role (ΔH_{act} = 13.7 kcal/mol, ΔG_{act} = 15.7 kcal/mol). On the ΔG scale, formation of **A8** thus remains as the rate-determining step of the induction phase, and the five-coordinate intermediates (**A8**, **A16**), formed in the latter part of the reaction, are entropically favored.

Considering the SBM catalytic cycle (Figure 11, red part) we first note that the overall reaction (**A16** + **R1** + **R2** → **A16** + **P1**, see Scheme 1) combines two reactant molecules into one product molecule so that the entropic contributions must be positive, which is indeed found (ΔH = −29.0 kcal/mol, $T\Delta S$ = 12.9 kcal/mol, ΔG = −16.1 kcal/mol). A similar reasoning applies to the intermediates in the SBM catalytic cycle (**A17** + **R1**, **A14** + **R1**, **A15**), all of which have fewer molecules than the entry point (**A16** + **R1** + **R2**). Therefore, in the ΔG profile of the catalytic cycle, all intermediates and the product are

shifted upward compared with the ΔH profile, but the other features remain qualitatively unchanged. In particular, the barriers of **A17** → **A14** and **A15** → **A16** remain similar on the ΔH and ΔG scales, and product formation remains as the rate-determining step. The qualitative conclusions drawn from the ΔH profile (Figure 11) thus remain valid also after taking entropic effects into account.

Conclusions

The reported comparison of the different reaction mechanisms involving **A1** has shown that the SBM mechanism provides the most favorable route to the hydrosilylation of **R2** by **R1**. The induction period of the catalyst involves the dissociation of a PPh_3 ligand, followed by a SBM reaction that results in the exchange of one of the chloride ligands with a hydride ligand. A subsequent isomerization from trigonal bipyramidal to square pyramidal by a shift of the hydride ligand yields the active form of the catalyst (**A16**). The activation enthalpy in the induction phase is 17.3 kcal/mol, corresponding to the exchange of the chloride ligand with a hydride ligand. This induction mechanism is clearly favored over the other alternative mechanisms tested for the following reasons: (1) the initial dissociation of a CO ligand is strongly disfavored as the enthalpy increases by 30.9 kcal/mol; (2) the exchange of the chloride ligand for a hydride via oxidative addition of the silane (i.e., **A2** → **A3**) causes a further destabilization of 16.3 kcal/mol (CO paths, Table 1); (3) the alternative coordination of vinylsilane (**R2**) and the subsequent addition of **R1** (OF mechanism) has a large barrier (32.1 kcal/mol) associated with the abstraction of the H atom from **R1**. Thus, the most favorable induction mechanism for **A1** to adopt an active catalytic form is via the initial abstraction of PPh_3 and the subsequent SBM reaction to replace the chloride ligand for a hydride.

This induction mechanism may generate the starting point of both the CH mechanism for the hydride−PPh_3 path (**A8**) or the SBM mechanism (**A16**). The initial coordination to the active species differs in the CH and SBM mechanisms: while the former involves the oxidative addition of **R1** in an endothermic reaction (9.0 kcal/mol, Table 1) via a high-energy TS (not located, Figure 4), the latter proceeds through a stabilizing η^2-coordination of **R2** (−16.0 kcal/mol, Table 2). The exothermicity of the reaction and the barrierless coordination of **R2** imply that the entry into the SBM pathway is preferred.

In the SBM catalytic cycle, the initial transformations (**A16** → **A17** → **A14** → **A15**) are facile. The final SBM step that generates the product (**A15** → **A16**) is rate-determining. The corresponding barrier of 21.8 kcal/mol is consistent with the experimentally observed activity.

Acknowledgment. We thank Dr. Hans-Jürgen Eberle for helpful discussions.

Supporting Information Available: Energy, thermochemical data, and Cartesian coordinates of all optimized structures and the complete ref 65 (PDF file). This material is available free of charge via the Internet at http://pubs.acs.org

OM060359H